Phase behavior of carbon dioxide + 2,4-dimethylpentane binary system at high pressures

Mihaela Ioniţă, Sergiu Sima, Adrian Crişciu, Catinca Secuianu, Dan Vladimir Nichita

The Journal of Supercritical Fluids 199 (2023) 105941

Contents lists available at ScienceDirect

The Journal of Supercritical Fluids

journal homepage: www.elsevier.com/locate/supflu

Phase behavior of carbon dioxide + 2,4-dimethylpentane binary system at high pressures

Mihaela Ioniţă [a], Sergiu Sima [a,*], Adrian Crişciu [a], Catinca Secuianu [a,b,**], Dan Vladimir Nichita [c,*]

[a] Department of Inorganic Chemistry, Physical Chemistry and Electrochemistry, Faculty of Chemical Engineering and Biotechnologies, University "Politehnica" of Bucharest, 1–7 Gh. Polizu Street, S1, 011061 Bucharest, Romania
[b] Department of Chemical Engineering, Imperial College London, South Kensington Campus, SW7 2AZ London, United Kingdom
[c] CNRS UMR 5150, Laboratoire des Fluides Complexes et leurs Réservoirs, Université de Pau et des Pays de l'Adour, 64013 Pau, France

HIGHLIGHTS

- Isothermal VLE data are for the first time reported for CO_2 + 2,4-dimethylpentane binary system at high-pressures.
- LV critical curve (P–T–X_1) is also measured at pressures up to 121.4 bar and 422.35 K.
- GEOS, PR, and SRK EoSs with classical van der Waals mixing rules successfully modeled the system.

GRAPHICAL ABSTRACT

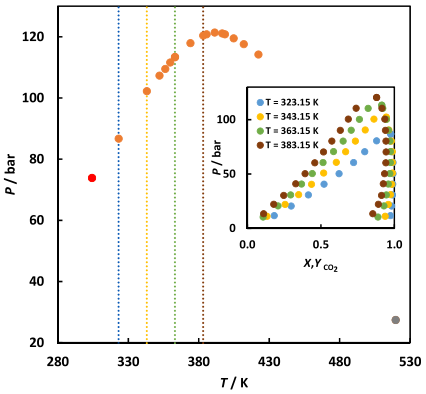

ARTICLE INFO

Keywords:
Carbon dioxide
2,4-Dimethylpentane
Phase equilibria
High-pressures
EoSs (GEOS, SRK, PR)

ABSTRACT

The phase behavior of the branched alkane 2,4-dimethyl pentane (2,4-DMP) and carbon dioxide (CO_2) binary mixture that has no published data, to the best of our knowledge, was studied. The liquid–vapor critical line was determined up to 121.4 bar and 422.35 K, as well as vapor–liquid equilibrium (VLE) data at different constant temperatures (323.15, 343.15, 363.15, and 383.15) K and pressures between (10.4 and 120.4) bar. Phase behavior investigation was carried out in a high-pressures (HP) cell fitted with a pair of sapphire windows, one acting as a piston, hence volume up to 60 cm^3, utilizing a static-analytical approach with phases sampling by the so called ROLSI valves (rapid online sample injectors) connected to a gas chromatograph (GC) for composition determination. The isothermal and critical data points for the carbon dioxide + 2,4-dimethylpentane binary mixture were modeled with the cubic equations of state (EoSs), i.e., Soave–Redlich–Kwong (SRK),

* Corresponding authors.
** Corresponding author at: Department of Inorganic Chemistry, Physical Chemistry and Electrochemistry, Faculty of Chemical Engineering and Biotechnologies, University "Politehnica" of Bucharest, 1–7 Gh. Polizu Street, S1, 011061 Bucharest, Romania.
E-mail addresses: sergiu.sima@upb.ro (S. Sima), catinca.secuianu@upb.ro, c.secuianu@imperial.ac.uk (C. Secuianu), dnichita@univ-pau.fr (D.V. Nichita).

https://doi.org/10.1016/j.supflu.2023.105941
Received 3 March 2023; Received in revised form 5 April 2023; Accepted 6 April 2023
Available online 8 April 2023

Peng–Robinson (PR), and General Equation of State (GEOS), in combination with van der Waals mixing rules (one- and two-parameter conventional mixing rules, 1PCMR and 2PCMR). The calculations demonstrated that the selected models are capable of correctly reproducing the phase behavior of the mixture under study.

1. Introduction

In the last years, we focused on examining the phase behavior of CO_2 and organic substances belonging to different classes that could be applied as physical solvents for carbon capture [1–3], CO_2 enhanced oil recovery and oil upstream treatment [4–6] or as substrates for clathrate hydrates, motivated by the increased interest on reducing the amount of CO_2 in the environment of the Earth. Moreover, the investigation of the phase behavior, thermodynamic or transport properties of carbon dioxide containing mixtures is essential in many other industries [7–10]. Among the organic substances studied as second component in carbon dioxide binary systems, despite their potential applications, some classes received less attention [11–15], particularly the carbon dioxide + branched *n*-alkane binary systems [16–19]. Our careful literature study revealed that, for instance, only for two, i.e., 3-methylhexane and 3, 3-dimethylpentane, of the eight position (chain) isomers of *n*-heptane + carbon dioxide binary systems, few equilibrium data are reported [20].

Because there are no data at HP for the binary mixture of CO_2 (1) + 2,4-DMP (2) in the public literature, we report here VLE data at constant temperature and the critical curve. 2,4-Dimethylpentane is a colorless liquid which is produced in high quantities in oil refineries, and it is blended with other gasoline components to give a high-octane fuel that allows combustion without knocking. It is also used for synthesizing auxiliary materials and resin fibers, in the binder and coating industry or as an intermediate and adhesive in oil drop coagulation thickener [21]. Besides the fundamental interest for studying new systems, the carbon dioxide + 2,4-dimethylpentane binary mixture can be utilized for investigating the hydrates formation and equilibrium, as promising results are obtained with 2,2-dimethylpentane [22,23].

In this study, VLE data (pressure – molar liquid and vapor compositions, *P – X, Y*) are reported for the CO_2 (1) + 2,4-DMP (2) binary mixture at the temperatures: 323.15 K, 343.15 K, 363.15 K, and 383.15 K and at pressures up to 121.4 bar (critical pressure maximum), along with the liquid–vapor critical line (pressure – temperature – composition).

The first data ever reported were modeled with the Soave–Redlich–Kwong (SRK) [24], Peng–Robinson (PR) [25] and General Equation of State (GEOS) [26–28] cubic equations of state (EoSs) and van der Waals mixing rules (one- and two-parameter conventional combining rules, 1PCMR and 2PCMR). These models were selected because, due to their simplicity and flexibility [29], cubic equations of state remain the favored method for simulating all types of mixtures, including complex systems like oil-based fluid [30–37]. The results by EoSs coupled with one-parameter conventional combining rules were also compared with the predictive group contribution method PPR78 model, wherein the first binary interaction parameter, k_{ij}, depends on temperature [16,17,36,38].

According to the categorization of phase diagrams provided by van Konyneburg and Scott [39] and reinterpreted by Privat and Jaubert [40], all three models chosen describe type II phase diagram (behavior). In the type II the *P-T* projection diagram binary systems present two critical curves, i.e., an unbroken liquid–vapor (LV) critical line linking the pure compounds' critical points and a second liquid–liquid (LL) critical line. The latter ends in a critical point called upper critical endpoint (UCEP) where is intersecting the three-phase liquid–liquid–vapor equilibrium (LLV) boundary. The chosen models calculated the UCEPs at very low temperatures below the triple point of carbon dioxide, which makes experimentally difficult the observation of the three-phase line occurrence.

In the pressure – temperature range studied in this work, experimental indication of type II phase behavior was not found. Although, the carbon dioxide + *n*-heptane system is type II phase behavior [41], the carbon dioxide + 2,4-DMP is type I phase behavior, as the branched alkane with the same number of carbon atoms is more soluble than the normal alkane.

2. Experimental section

2.1. Materials

Carbon dioxide (mass fraction purity min. 0.99995) was acquired from Linde (Linde Gaz Romania), while 2,4-dimethylpentane (mass fraction purity higher than 0.99) was bought from Sigma-Aldrich (25 g bottles), as summarized in Table 1. Both chemicals were employed without additional purification. However, the stated concentration of 2,4-dimethylpentane was verified and confirmed by using gas chromatographic analysis for each bottle used.

2.2. Apparatus and procedure

Both isothermal and critical curve experiments were done using the same high-pressures (HP) rig described thoroughly in earlier publications [42–45]. The static-analytical procedure with both phases (liquid, *L* and vapor, *V*) sampling is used to measure the vapor–liquid equilibrium at constant temperatures, which, according to refs. [11–15,46], it can be summarized as *AnTVisVarCap*. The equilibrium cell fitted with an opposite pair of sapphire windows, one acting as a piston, is the principal module of the phase equilibrium installation. The HP cell is connected via capillaries with a sampling module and an analyzing system [45], as well as with a Teledyne Isco pump, model 500D, for charging the carbon dioxide. The sampling module contains a pair of HP electromechanical valves for sampling, i.e., the rapid online sampler injectors called ROLSI™ that were made by the Center énergétique et proceeds of the MINES ParisTech/CEP-TEP (Fontainbleau, France) [47]. The liquid samples are very quickly vaporized in the expansion compartment of the corresponding sampler injector that is heated up with a heating system (electric resistance). The ROLSI valves are also connected using capillaries thermally insulated and heated by a linear resistor, which is connected to a regulator (Armines/CEP/TEP), to a gas chromatograph (GC). The GC made by Perichrom (France) is fitted out with a detector, i.e., thermal conductivity detector (TCD). The HP-Plot/Q column inside of the GC is 30 m long and has a diameter of 0.530 mm. The carrier gas used in the GC is helium and its flow rate is 30 mL/min.

The same experimental procedure was employed as in our previous

Table 1
Description of substances.

Substance	Chemical formula	CAS Registry Number	Manufacturer	Purification method	Minimum mass fraction purity
Carbon dioxide	CO_2	124–38–9	Linde	None	0.99995
2,4-Dimethylpentane (2,4-DMP)	C_7H_{16}	108–08–7	Sigma-Aldrich	None	0.99

papers [1,18,48–50]. Briefly, the apparatus's complete internal loop, as well as the HP equilibrium visual cell, is repeatedly purged with CO_2 before being evacuated with the use of a vacuum pump. In the equilibrium cell is then loaded the 2,4-DMP that already was degassed with a vacuum pump and strong mixing. The CO_2 is loaded in the HP equilibrium cell employing the syringe pump from Teledyne Isco and the pressure is adjusted to the chosen value while strongly mixing. At this point, the HP cell is heated up to the intended working temperature. The mixture in the HP cell is continually agitated for a couple of hours to attain equilibrium conditions. After roughly an hour, the stirrer is turned off to allow full separation of the coexisting phases. Very small amounts from both the liquid and the vapor phases are drawn with the ROLSI valves and put through a gas chromatograph analysis. At least six liquid phase samples are routinely analyzed to ensure reproducibility at the equilibrium pressure and temperature. The equilibrium pressure inside the HP cell does not change, due to the small sample amounts.

Utilizing the proper chromatographic syringes and known dosages of each chemical, the TCD is calibrated for carbon dioxide and 2,4-dimethylpentane. In order to determine the component's mole number in relation to the chromatographic area, calibration data are correlated to quadratic polynomials. The gas chromatograph calibration curves have the Pearson coefficients of 0.9999 for CO_2 and 0.9986 for 2,4-DMP.

It was previously explained how to estimate the uncertainty in all variables and properties [51,52]. The platinum temperature sensor attached to a device with digital display was calibrated at the Romanian Bureau of Legal Metrology using a digital accurate thermometer with a PT 100 sensor. The uncertainty of the platinum probe is assessed to be within ± 0.1 K as explained in ref. [51]. The model 580 C hydraulic dead-weight accurate comparator made by DH-Budenberg SA (Aubervilliers, France) was employed to calibrate the pressure transducer which is attached to a digital multimeter. The uncertainty of the pressures is assessed, as explained in [53], to be within ± 0.015 MPa for a pressure span between 0.5 and 20 MPa.

The experimental method to determine critical points is as follows [54]. Starting with a homogenous phase, the composition is examined while the temperature and pressure are randomly chosen for the measurement. By gradually changing the cell's volume with the manual pump, the pressure is adjusted to see if a dew- (DP) or a bubble-point (BP) is produced. In the case that a BP is noticed visually, the temperature is gradually raised until the first DP appears, at which time the pressure is elevated to a homogenous phase while the composition is obtained through sampling. Then, once the first liquid drops are seen, the pressure will be gradually decreased. At this moment, the temperature is gradually lowered at the same time with decreasing the volume for the system to be at the boundary between the single phase (homogeneous domain) and two-phases state (heterogeneous domain). The reducing of temperature carries on up to the first gas bubbles are noticed. The process is subsequently remade while cooling gradually and adding fresh quantities of CO_2.

3. Modeling

The phase behavior of the CO_2 (1) + 2,4-DMP (2) binary mixture was modeled with the SRK [24], PR [25], and GEOS [26–28] cubic EoSs together with van der Waals combining rules (one- and two-parameter conventional mixing rules, 1PCMR and 2PCMR).

The GEOS [26–28] equation of state is:

$$P = \frac{RT}{V-b} - \frac{a(T)}{(V-d)^2 + c} \tag{1}$$

with the classical van der Waals mixing rules

$$a = \sum_i \sum_j X_i X_j a_{ij} \tag{2}$$

$$b = \sum_i \sum_j X_i X_j b_{ij} \tag{3}$$

$$c = \sum_i \sum_j X_i X_j c_{ij} \tag{4}$$

$$d = \sum_i X_i d_i \tag{5}$$

and the combination rules for a_{ij}, b_{ij}, and c_{ij}

$$a_{ij} = \left(a_i a_j\right)^{\frac{1}{2}}\left(1 - k_{ij}\right) \tag{6}$$

$$b_{ij} = \frac{b_i + b_j}{2}\left(1 - l_{ij}\right) \tag{7}$$

$$c_{ij} = \pm\left(c_i c_j\right)^{\frac{1}{3}} \tag{8}$$

with "+ " for c_i, $c_j > 0$ and "–" for c_i, $c_j < 0$. The c parameter of pure compounds typically has negative values.

For a pure component, the four parameters (a, b, c, and d) are stated as follows:

$$a(T) = \frac{R^2 T_c^2}{P_c}\beta(T_r)\Omega_a \tag{9}$$

$$b = \frac{RT_c}{P_c}\Omega_b \tag{10}$$

$$c = \frac{R^2 T_c^2}{P_c^2}\Omega_c \tag{11}$$

$$d = \frac{RT_c}{P_c}\Omega_d \tag{12}$$

Four critical conditions are set, with $\alpha_c$as the Riedel criterion:

$$P_r = 1 \tag{13}$$

$$\left(\frac{\partial P_r}{\partial V_r}\right)_{T_r} = 0 \tag{14}$$

$$\left(\frac{\partial^2 P_r}{\partial V_r^2}\right)_{T_r} = 0 \tag{15}$$

$$\alpha_c = \left(\frac{\partial P_r}{\partial T_r}\right)_{V_r} \tag{16}$$

at $T_r = 1$ and $V_r = 1$, the equations of the parameters Ω_a, Ω_b, Ω_c, Ω_d are found:

$$\Omega_a = (1 - B)^3 \tag{17}$$

$$\Omega_b = Z_c - B \tag{18}$$

$$\Omega_c = (1 - B)^2(B - 0.25) \tag{19}$$

$$\Omega_d = Z_c - \frac{(1 - B)}{2} \tag{20}$$

$$B = \frac{1 + m}{\alpha_c + m} \tag{21}$$

whereZ_c is the critical compressibility factor and P_r, T_r, V_r are the reduced variables.

The function used for the temperature is:

$$\beta(T_r) = T_r^{-m} \tag{22}$$

By constraining the equation of state to replicate the experimental

Table 2
Pure substances properties [58].

Substances	Critical temperature T_c/K	Critical pressure P_c/bar	Critical volumen V_c/cm·mol^{-1}	Acentric factor ω
Carbon dioxide	304.21	73.83	93.90	0.223621
2,4-Dimethylpentane	519.80	27.40	418.00	0.302248

vapor pressures and liquid volumes on the saturation curve spanning from the triple point to the critical point, the m and α_c parameters of the GEOS were computed [55].

The Soave–Redlich–Kwong [24] equation of state is:

$$P = \frac{RT}{V-b} - \frac{a(T)}{V(V+b)} \tag{23}$$

With the two constants, a and b:

$$a = 0.42748\frac{R^2T_c^2}{P_c}\alpha(T) \tag{24}$$

$$b = 0.08664\frac{RT_c}{P_c} \tag{25}$$

$$\alpha(T_R,\omega) = \left[1 + m_{SRK}\left(1 - T_R^{0.5}\right)\right]^2 \tag{26}$$

$$m_{SRK} = 0.480 - 1.574\omega - 0.176\omega^2 \tag{27}$$

The Peng–Robinson [25] equation of state is:

$$P = \frac{RT}{V-b} - \frac{a(T)}{V(V+b)+b(V-b)} \tag{28}$$

with the two constants, a and b:

$$a = 0.45724\frac{R^2T_c^2}{P_c}\alpha(T) \tag{29}$$

Table 3
Pressures (P) – compositions (X_1, Y_1 – mole fractions of component 1 in the liquid phase and vapor phase respectively) at various temperatures (T) for the binary system CO_2 (1) + 2,4-DMP (2).

P/bar	X_1	Y_1	P/bar	X_1	Y_1
T/K = 323.15 ± 0.1					
11.6	0.1825	0.9736	60.5	0.7224	0.9904
20.5	0.2980	0.9815	70.5	0.7981	0.9832
30.7	0.4143	0.9874	80.5	0.8791	0.9741
40.6	0.5214	0.9894	86.7[a]	0.9755	0.9755
50.3	0.6238	0.9908			
T/K = 343.15 ± 0.1					
11.1	0.1336	0.9378	70.5	0.6687	0.9854
22.0	0.2566	0.9590	80.3	0.7346	0.9795
31.0	0.3481	0.9737	90.5	0.8015	0.9626
40.5	0.4364	0.9817	100.5	0.8612	0.9463
50.8	0.5187	0.9862	102.2	0.9445	0.9445
60.7	0.6043	0.9863			
T/K = 363.15 ± 0.1					
10.4	0.1071	0.8887	70.6	0.5857	0.9731
20.6	0.2080	0.9288	80.2	0.6512	0.9699
30.7	0.2941	0.9454	90.2	0.7060	0.9597
40.7	0.3685	0.9593	100.2	0.7621	0.9459
50.4	0.4415	0.9692	110.4	0.8214	0.9214
60.5	0.5147	0.9727	113.3	0.9143	0.9143
T/K = 383.15 ± 0.1					
13.4	0.1108	0.8535	70.3	0.5183	0.9432
22.1	0.1791	0.8907	80.2	0.5744	0.9427
30.2	0.2474	0.9123	90.1	0.6320	0.9395
41.0	0.3291	0.9243	100.5	0.6865	0.9345
50.2	0.3921	0.9331	110.5	0.7401	0.9153
60.3	0.4586	0.9418	120.4	0.8787	0.8787

Standard uncertainties: $u(T)$ = 0.1 K, $u(P)$ = 0.1 bar, $u(X_1)$ = 0.001, $u(Y_1)$ = 0.005

$$b = 0.077796\frac{RT_c}{P_c} \tag{30}$$

$$\alpha(T_R,\omega) = \left[1 + m_{PR}\left(1 - T_R^{0.5}\right)\right]^2 \tag{31}$$

$$m_{PR} = 0.37464 - 1.54226\omega - 0.26992\omega^2 \tag{32}$$

The two-parameter conventional (2PCMR) combining rules are expressed by the following:

$$a = \sum_i\sum_j X_iX_ja_{ij} \tag{33}$$

$$b = \sum_i\sum_j X_iX_jb_{ij} \tag{34}$$

with a_{ij} and b_{ij} as in Eqs. (6) and (7).

The critical curve of the mixture also was calculated with the PPR78 model [36–38,56], which is based on the original form of the Peng-Robinson EoS and a predictive k_{ij} temperature-dependent (Eq. (4) in ref. [37]).

The original form of the temperature function $\alpha(T_r)$ was used for all three models, though in a recent paper [57] a version of the generalized Soave α-function was proposed, suitable for the Peng–Robinson and Soave-Redlich–Kwong equations of state.

The critical parameters as well as the acentric factors of the two pure compounds utilized in the computations are presented in Table 2. In recent papers [1,2,48], it was shown that the choice of critical parameters and acentric factors of pure compounds are important, but in this case the values for the 2,4-DMP branched alkane are similar in different databases. Therefore, we chose the values given in the DIPPR database [58], as recommended in other papers [59,60].

The modeling approach for the carbon dioxide + 2,4-DMP was threefold steps. Firstly, the experimental data at each temperature were correlated with all three EoSs, coupled with one-parameter conventional mixing rules, 1PCMR. The optimized values of binary interaction parameter k_{ij} calculated for each of the four measured temperatures were averaged and this value was then used to model the critical curves. The critical curve was also calculated with the PPR78 model [38] and compared with the SRK, GEOS, and PR results. Secondly, the experimental data were fitted with GEOS, PR, and SRK and two-parameter conventional mixing rules, 2PCMR. The binary interaction parameters (BIPs), k_{ij} and l_{ij}, are calculated by minimizing the next objective function:

$$F_{ob} = \sum_{i=1}^{N}\left(\frac{P_i^{exp} - P_i^{calc}}{P_i^{exp}}\right)^2 \tag{35}$$

The optimized values of the binary interaction parameters, k_{ij} and l_{ij}, at each temperature and for each model were averaged and the median values were used to model the critical curves.

For the Peng–Robinson model, we compared both bubble point pressures [51] and flash calculations. In the latter case, phase diagrams were generated by successive T, P–flash calculations, using the Peng–Robinson equation of state, combined with a two-parameter van der Waals-type mixing rule as the underlying thermodynamic model. The pressure step between successive tie-lines was adjusted proportionally to the tie-line length, in order to achieve better resolution near the critical point. Binary interaction parameters were simultaneously fitted to all four isotherms (57 experimental tie-lines in total). To this end, the

Table 4
Critical line for CO_2 (1) + 2,4-DMP (2).

T/K	P/bar	X_1	T/K	P/bar	X_1
519.80[a]	27.4	0.0000	374.15	117.9	0.8946
422.35	114.2	0.7239	363.15[b]	113.4	0.9144
411.95	117.6	0.7587	363.05	113.3	0.9143
404.75	119.5	0.7887	359.75	111.6	0.9201
398.55	120.8	0.8182	356.25	109.5	0.9248
396.65	121.1	0.8237	352.15	107.3	0.9305
391.35	121.4	0.8519	343.15[b]	102.2	0.9445
385.55	120.8	0.8734	323.15[b]	86.7	0.9755
383.15[b]	120.4	0.8787	304.21	73.83	1.0000

Standard uncertainties: $u(T) = 0.1$ K, $u(P) = 0.1$ bar, $u(X_1) = 0.001$;
[a] DIPPR [58] values;
[b] interpolated values.

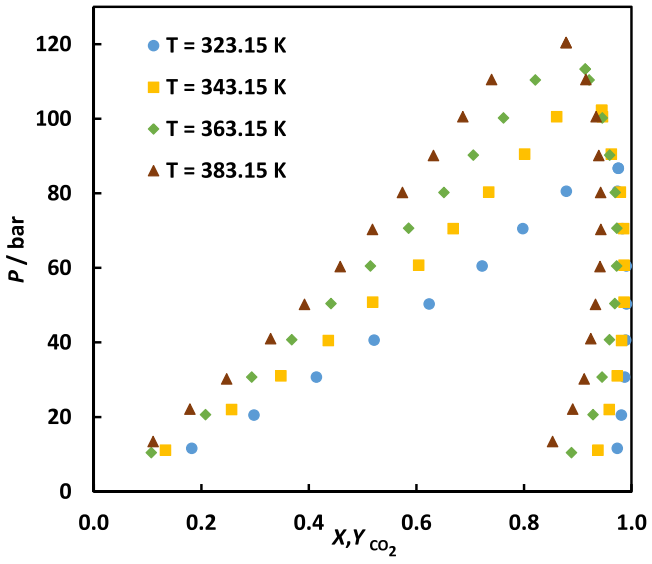

Fig. 1. Pressure-composition data for CO_2 (1) + 2,4-DMP (2) at different temperatures.

implicit objective function, Eq. (36) below, firstly suggested by Englezos [61], was optimized using a self-adaptive differential evolution algorithm [62,63] in order to avoid premature convergence to a sub-optimal parameter set:

$$F(k_{ij}, l_{ij}) = \sum_{i=1}^{N_{exp}} \sum_{j=1}^{N} \left(X_{ji}\phi_{ji}^{L} - Y_{ji}\phi_{ji}^{V} \right)^2 \quad (36)$$

where N is the number of components (2), and N_{exp} is the number of experimental points.

Lastly, we calculated the critical curves using a temperature-dependent k_{ij} [64] and a constant l_{ij} for all three EoSs and the corresponding isothermal pressure-composition diagrams.

The computations were made using our internal software tool entitled "**Ph**ase **Eq**uilibria Database and Applications – ***PHEQ***" [65] and with "Global Phase Equilibrium Calculations – GPEC" software [64, 66–68]. The critical lines were calculated with the CRITHK dedicated module of *PHEQ,* in which the technique given by Heidemann and Khalil [69] with the numerical derivatives provided by Stockfleth and Dohrn [70] is implemented, the in-house software developed by [71], and GPEC.

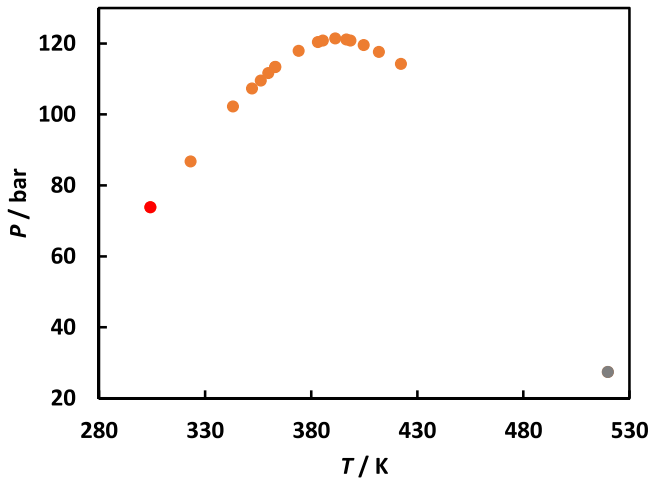

Fig. 2. *P–T* fluid phase diagram of the CO_2 (1) + 2,4-DMP system: ●, critical point of CO_2; ●, critical point of 2,4-DMP; ●, experimental LV critical curve, this work.

Table 5
GEOS, PR, and SRK/1PCMR modeling results for the CO_2 + 2,4-DMP binary system.

EoS/ Mixing rule	T/K	k_{12}	F_{ob}	N_{exp}	N_{conv}	AADP/ %	AADY/ %
GEOS/ 1PCMR	323.15	0.0000	0.0156	8	8	4.03	0.87
	343.15	0.0003	0.0203	10	10	3.82	2.00
	363.15	–0.0069	0.0405	11	11	5.27	3.46
	383.15	–0.0059	0.0343	11	11	4.41	5.02
		–0.0031				**4.38**	**2.84**
PR/ 1PCMR	323.15	0.0202	0.0128	8	8	3.65	0.63
	343.15	0.0212	0.0130	10	10	3.14	1.19
	363.15	0.0125	0.0262	11	11	4.34	1.85
	383.15	0.0149	0.0179	11	11	3.27	2.75
		0.0172				**3.60**	**1.61**
SRK/ 1PCMR	323.15	0.0256	0.0124	8	8	3.58	0.59
	343.15	0.0278	0.0125	10	10	3.10	1.09
	363.15	0.0202	0.0251	11	11	4.25	1.62
	383.15	0.0245	0.0162	11	11	3.12	2.27
		0.0245				**3.51**	**1.39**

4. Results and discussion

4.1. Experimental results

VLE data (*P–X, Y*) for the CO_2 + 2,4-DMP binary mixture were experimentally determined at four temperatures (323.15 K, 343.15 K, 363.15 K, and 383.15 K), and in the pressure range spanning from 10.4 to 120.4 bar. The isotherms are shown in Table 3, and mole fractions are represented with four significant figures, as resulted from the uncertainties calculation [4,51,53]. The critical curve was also examined beginning at the CO_2 critical point and continuing up to 422.35 K. The greatest pressure, which corresponds to the critical pressure maximum (CPM), was 121.4 bar. The results are shown in Table 4 together with their standard uncertainties evaluated as explained in ref. [72].

Fig. 1 illustrates the isotherms determined in this study located in the supercritical region of CO_2, while Fig. 2 depicts the *P–T* projection of the experimental critical line.

4.2. Modeling results with GEOS/1PCMR, SRK/1PCMR, and PR/1PCMR

The isothermal data were correlated with SRK, GEOS, and PR/1PCMR using the critical parameters and acentric factors provided

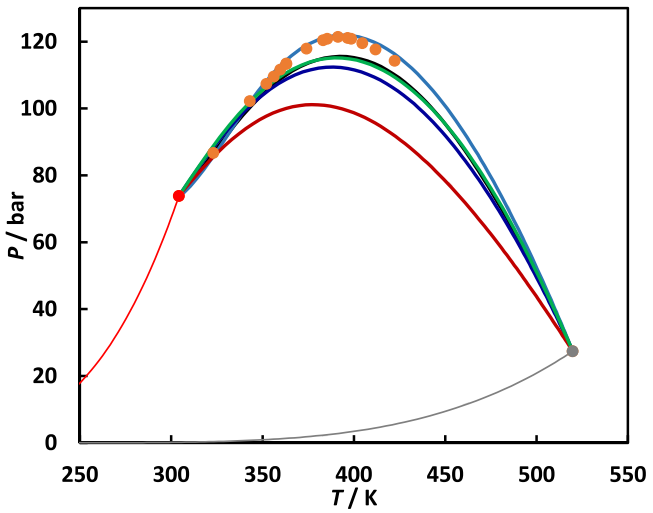

Fig. 3. *P–T* fluid phase diagram of the carbon dioxide (1) + 2,4-dimethylpentane system. (●), critical point of CO_2; (●), critical point of 2,4-DMP; (–), vapor pressure of CO_2; (–), vapor pressure of 2,4-DMP; (●), experimental liquid-vapor critical curve; ( ), GEOS/1PCMR (k_{ij} = -0.0031); ( ), PR/1PCMR (k_{ij} = 0.0172); ( ), SRK/1PCMR (k_{ij} = 0.0245); (■), PPR78; ( ), PR/1PCMR (k_{ij} = 0.1200).

DIPPR database [58] (Table 2) and the results are presented in Table 5. The average absolute deviations in bubble-point pressures (AADP, %) and the average absolute deviations in the vapor-phase compositions (AADY, %) are determined using the following equations:

$$AADP\left(\%\right) = \frac{1}{N_{\exp}} \sum_{i=1}^{N_{\exp}} \left| \frac{P_i^{\exp} - P_i^{calc}}{P_i^{\exp}} \right| \times 100 \tag{25}$$

$$AADY\left(\%\right) = \frac{1}{N_{\exp}} \sum_{i=1}^{N_{\exp}} \left| Y_i^{\exp} - Y_i^{calc} \right| \times 100 \tag{26}$$

The smallest errors both in bubble-point pressures and vapor-phase compositions are achieved with SRK/1PCMR, followed closely by PR/1PCMR, and the largest ones are obtained with the GEOS/1PCMR model (Fig. 1S.–5S., Supplementary information). While the calculation results cannot be distinguished in the liquid phase compositions up to medium pressures for all three models at each temperature, the differences in the vapor curves are clearer (Fig. 2S. – 5S.) It should be remarked that though the AADP, % and AADY, % have the highest values for GEOS, the average value of the binary interaction parameter is the smallest for this model of the three chosen. The average values of the binary interaction parameter, k_{ij}, together with the AADP, % and AADY, % for each model are shown in bold in Table 5. The corresponding minimum scores for the objective function (F_{ob}), the number of experimental points (N_{exp}), and the number of convergent points (N_{conv}) are also reported in Table 5. The average k_{ij} was used to calculate the critical line of the system, as shown in Fig. 3. Moreover, the experimental critical curve measured in this work and the results by the three EoSs coupled with one-parameter conventional mixing rule considered are compared in the *P–T* diagram with the predictive model PPR78 [16,17,38]. It can be easily seen that the critical pressure maximum is underestimated for all models, in the order GEOS < PR < SRK ≈ PPR78, the last two behaving similarly and being the closest to the experimental data.

The temperatures corresponding to the critical pressure maximum are shifted to the left as compared with the experimental for all models, the smallest difference being recorded for SRK and PPR78. As differences in the experimental and calculated critical pressure maximum vary between (–20.26 and –5.84) bar and between (–14.42 and 0.71) K in the corresponding temperatures, we used a trial-and-error procedure and we found that for the PR/1PCMR model with a constant k_{ij} = 0.12 a very good critical behavior (light blue curve in Fig. 3.) can be obtained in the *P–T* projection. It should be noted that all models with one-conventional binary interaction parameter mixing rule lead also to a type II phase behavior. However, when plotting the calculation results in the *P–X*$_1$ and *T–X*$_1$ projections, it is obvious that the three EoSs combined with one parameter conventional mixing rule or the PPR78 model are not accurate enough for this system (Fig. 4).

In both cases, the closest qualitative behavior to the experimental one is obtained with SRK equation of state, while for the PR with constant k_{ij} = 0.12, though the CPM value is very close to the experimental one, it can be observed that the composition corresponding to the CPM is significantly shifted to the left compared with the experimental one.

Therefore, in the next step we fitted the isothermal experimental data using the GEOS, PR, and SRK EoSs coupled with two-conventional parameters mixing rules, 2PCMR.

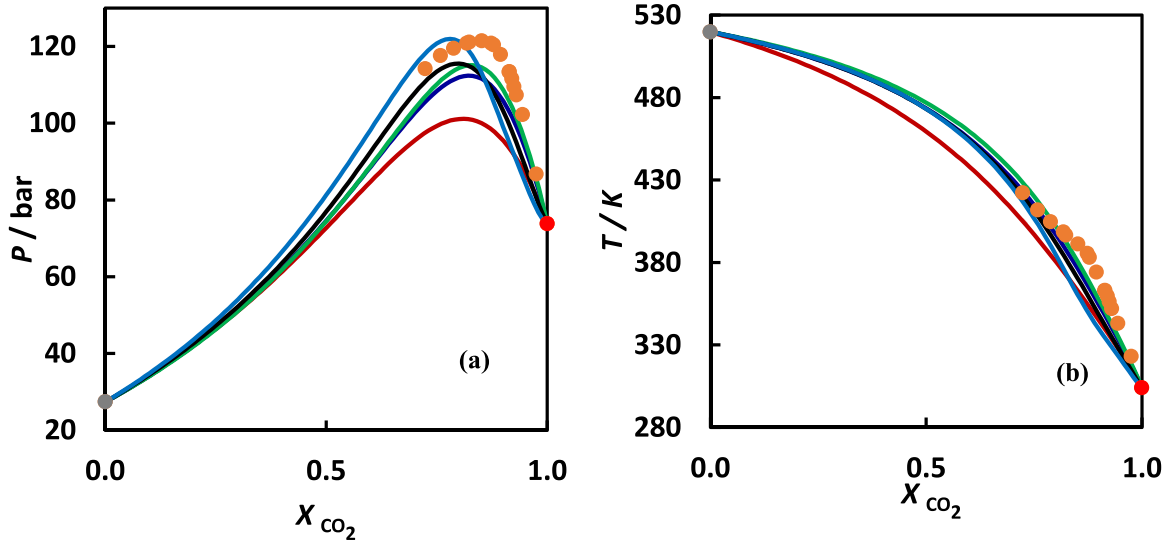

Fig. 4. *P–X*$_1$ **(a)** and *T–X*$_1$ **(b)** projections of the critical curve of the CO_2 + 2,4-DMP binary system. (●), critical point of CO_2; (●), critical point of 2,4-DMP; (–), vapor pressure of CO_2; (–), vapor pressure of 2,4-DMP; (●), experimental liquid-vapor critical curve; ( ), GEOS/1PCMR (k_{ij} = -0.0031); ( ), PR/1PCMR (k_{ij} = 0.0172); ( ), SRK/1PCMR (k_{ij} = 0.0245); (■), PPR78; ( ), PR/1PCMR (k_{ij} = 0.1200).

Table 6
GEOS, PR, and SRK EoSs coupled with two-conventional mixing rules modeling results for the CO_2 + 2,4-DMP binary system.

EoS/Mixing rule	T/K	k_{12}	l_{12}	F_{ob}	N_{exp}	N_{conv}	AADP/%	AADY/%
GEOS/2PCMR	323.15	0.0213	0.0204	0.0014	8	8	1.16	0.82
	343.15	0.0177	0.0192	0.0046	10	10	1.62	1.93
	363.15	0.0122	0.0232	0.0027	11	11	1.34	3.86
	383.15	0.0148	0.0275	0.0047	11	11	1.55	4.47
		0.0165	**0.0226**				**1.42**	**2.77**
PR/2PCMR	323.15	0.0533	0.0373	0.0010	8	8	1.05	0.57
	343.15	0.0481	0.0322	0.0015	10	10	0.93	1.06
	363.15	0.0498	0.0445	0.0024	11	11	1.27	1.66
	383.15	0.0485	0.0416	0.0015	11	11	0.86	2.29
		0.0499	**0.0389**				**1.03**	**1.40**
SRK/2PCMR	323.15	0.0585	0.0373	0.0010	8	8	1.03	0.53
	343.15	0.0553	0.0328	0.0014	10	10	0.89	1.00
	363.15	0.0570	0.0443	0.0024	11	11	1.27	1.36
	383.15	0.0566	0.0406	0.0014	11	11	0.78	1.89
		0.0569	**0.0388**				**0.99**	**1.20**

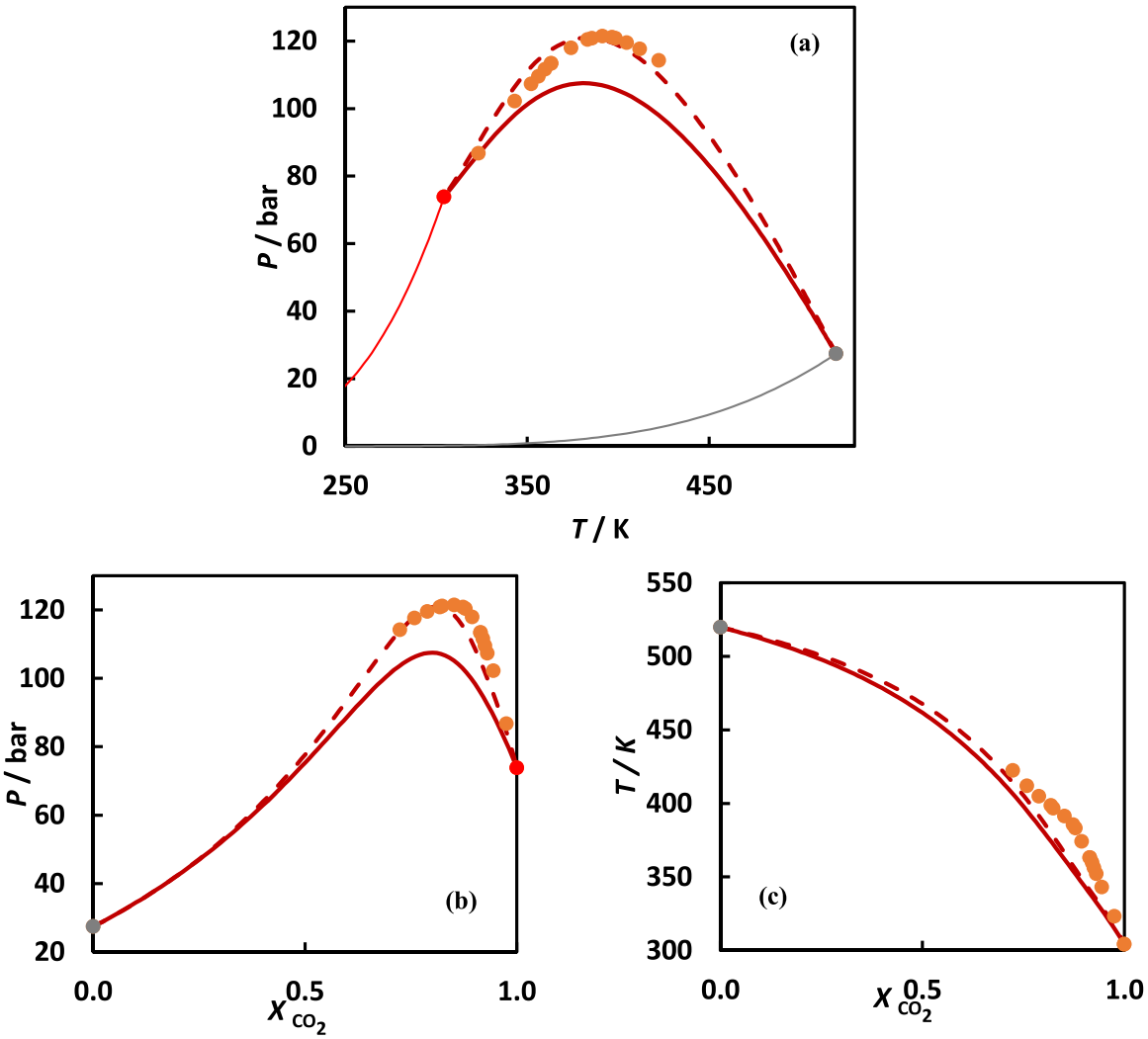

Fig. 5. *P–T* (**a**), *P–X*$_1$ (**b**), and *T–X*$_1$ (**c**) fluid phase diagram of the carbon dioxide (1) + 2,4-dimethylpentane (2) binary system. (●), critical point of CO_2; (●), critical point of 2,4-DMP; (–), vapor pressure of CO_2; (–), vapor pressure of 2,4-DMP; (●), experimental LV critical curve; (▪), GEOS/2PCMR (k_{ij} = 0.0165; l_{ij} = 0.0226); (▪ ▪), GEOS/2PCMR (k_{ij} = f (*T*); l_{ij} = 0.0701).

4.3. GEOS/2PCMR, PR/2PCMR, and SRK/2PCMR results

The experimental isothermal data were regressed with GEOS, PR, and SRK equations of state coupled with classical van der Waals mixing rules with two binary interaction parameters (BIPs) and the results are plotted in Fig. 6S.–9S. An example of the optimization result using classical van der Waals mixing rules with one- and two-conventional parameters is shown in Fig. 10S. As temperature increases, the modeling results are improved for the 2PCMR mixing rule. The correlation results are shown in Table 6. The meaning of the data presented in

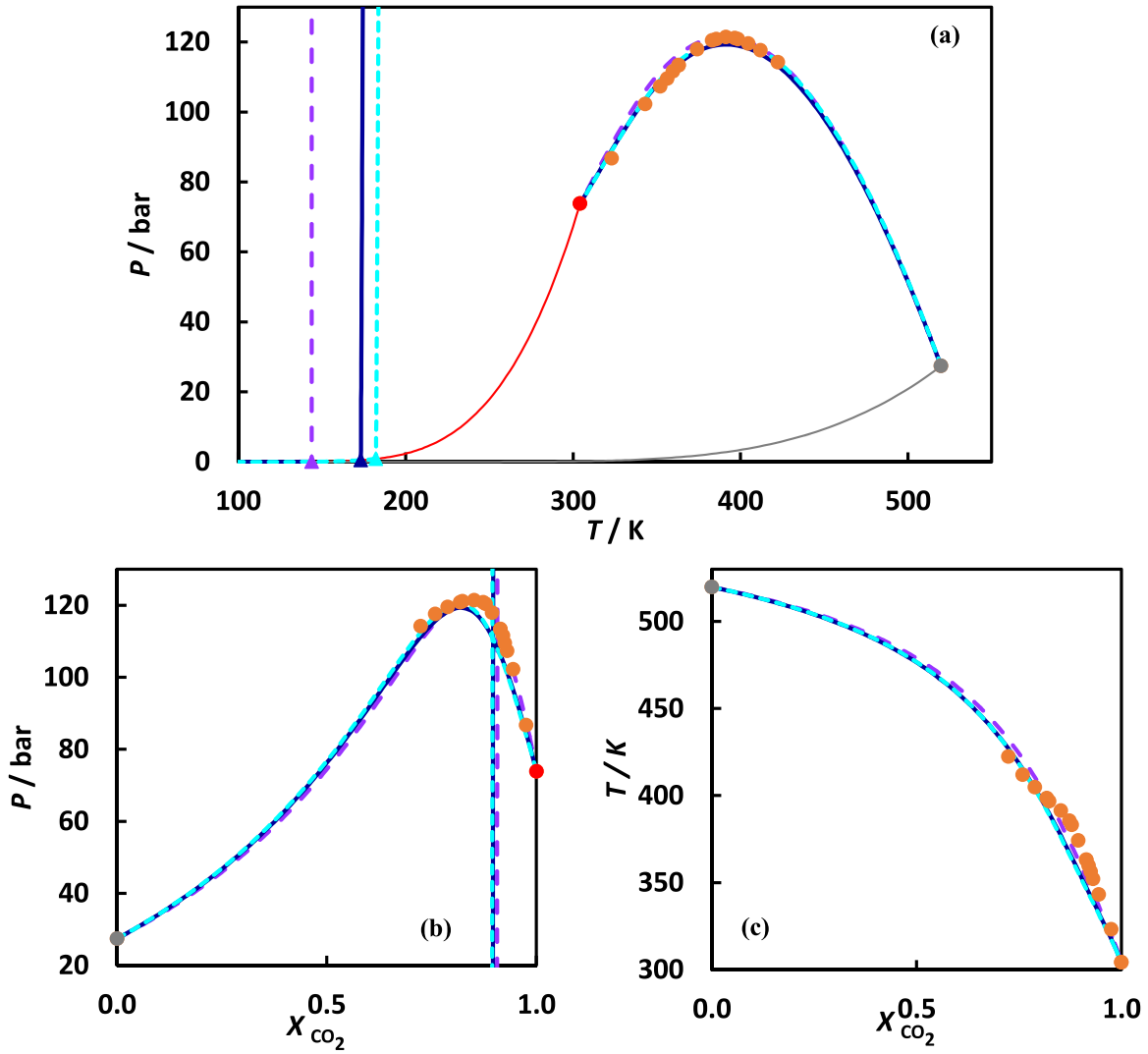

Fig. 6. *P–T* (**a**), *P–X*$_1$ (**b**), and *T–X*$_1$ (**c**) phase diagrams of the CO_2 (1) + 2,4-DMP (2) binary system. (●), CO_2 critical point; (●), 2,4-DMP critical point; (–), CO_2 vapor pressure; (–), 2,4-DMP vapor pressure; (●), experimental LV critical curve; (▬; ▲), PR/2PCMR (k_{ij} = 0.0499; l_{ij} = 0.0389); (▬ ▬; ▲), PR/2PCMR (k_{ij} = f (*T*); l_{ij} = 0.0640); (- - - -; ▲), PR/2PCMR (k_{ij} = 0.060390; l_{ij} = 0.042365). The critical curves (LV and LL) are plotted with tick full and dashed lines and the UCEPs are drawn with triangles.

this table is similar to that presented for modeling with one parameter, with the exception of the binary interaction parameter, l_{ij}. Both errors in pressure and vapor phase compositions decreased for all three selected models and the trend noticed for one-conventional parameter mixing rule is comparable, i.e., the best performance was achieved by SRK/2PCMR, followed by PR/2PCMR, and GEOS/2PCMR, with the observation that the differences in the model results are smaller. The optimized values of the binary interaction parameters, k_{ij} and l_{ij}, are averaged for each equation of state (presented in bold in Table 6) and these values were used to calculate the critical curves. All three models lead to type II phase behavior and the calculated UCEPs are situated at very low temperatures, less than 200 K which is below the triple point of CO_2. At such low temperatures the occurrence of the three-phase equilibrium line is almost impossible to be observed experimentally as it could be masked by a solid-liquid equilibrium curve, which is beyond the scope of this paper and beyond the reach of our experimental setup.

In Fig. 5–7 are presented all three projections (*P–T* (**a**), *P–X*$_1$ (**b**), and *T–X*$_1$ (**c**)) of the phase behavior of the CO_2 + 2,4-DMP system, i.e., critical curves (liquid–vapor, LV, and liquid–liquid, LL), the equilibrium three-phases lines (LLV), and upper critical endpoints (UCEPs) by the three models in comparison with the experimental data. The calculation results with average values of the BIPs are shown as full lines in each figure (GEOS – dark red; SRK – green; PR – dark blue). As expected, the experimental LV critical curve in the *P–T* projection is best reproduced by SRK, while PR is slightly underestimating the CPM (~ 2 bar) and GEOS is calculating the CPM at 107.51 bar (Fig. 11S).

However, the critical composition corresponding to the CPM is undervalued by all three models, while the critical temperature is much smaller than the experimental one for GEOS and higher for both SRK and PR, which is reflected in the *P–X*$_1$, and *T–X*$_1$ projections (Fig. 5–7 and Fig. 12S and 13S).

While in Fig. 5–7 are compared the experimental LV critical data and the calculation results separately for each model, in Fig. 11S. - 13S. the experimental data are plotted together with all three EoSs in the corresponding projection.

Fig. 5 shows the results by GEOS model with the average values of

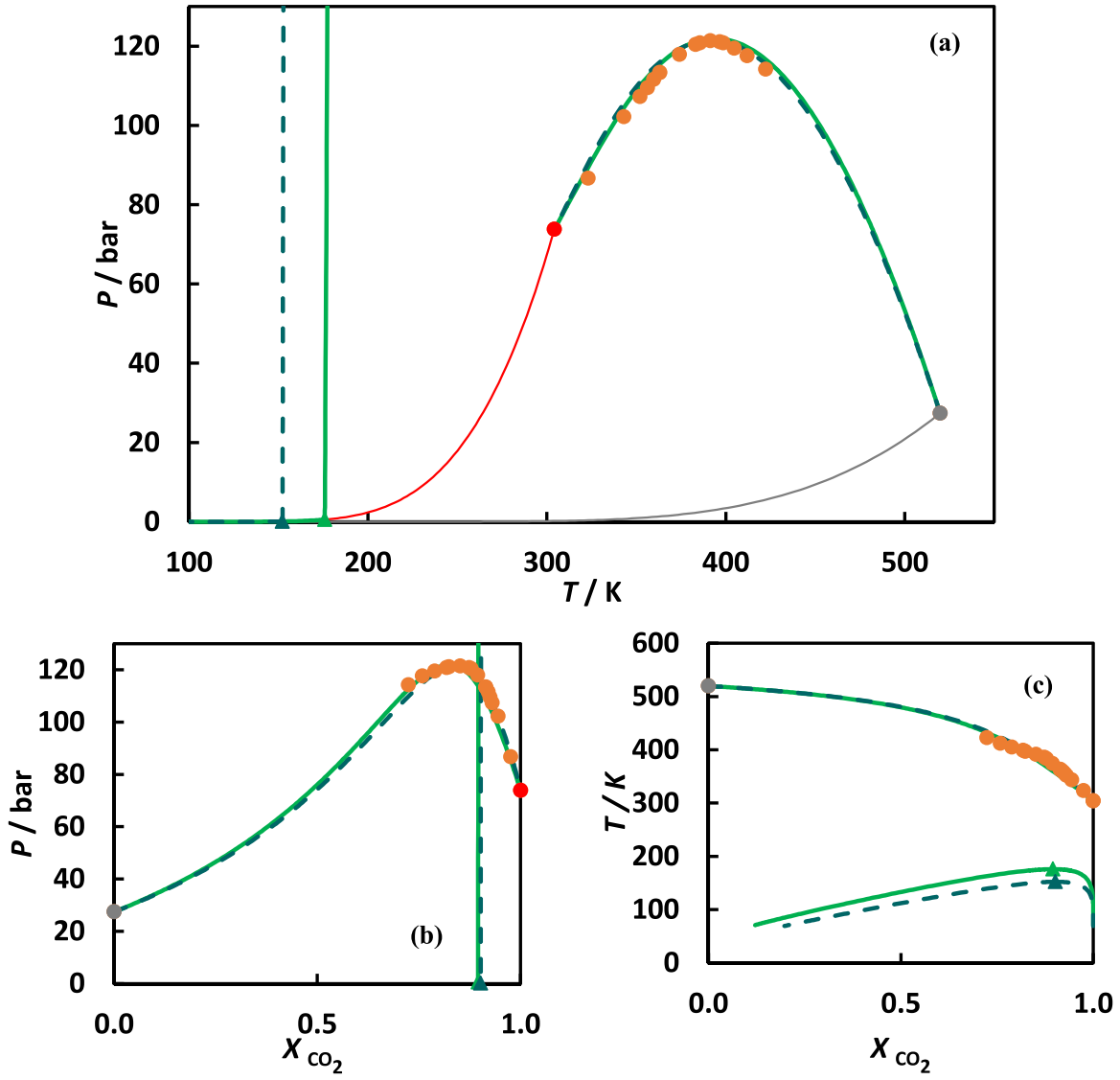

Fig. 7. *P–T* (**a**), *P–X*$_1$ (**b**), and *T–X*$_1$ (**c**) phase diagrams of the CO_2 (1) + 2,4-DMP (2) binary system. (●), CO_2 critical point; (●), 2,4-DMP critical point; (–), CO_2 vapor pressure; (–), 2,4-DMP vapor pressure; (●), experimental LV critical curve; (—; ▲), SRK/2PCMR (k_{ij} = 0.0569; l_{ij} = 0.0388); (— —; ▲), SRK/2PCMR (k_{ij} = f (*T*); l_{ij} = 0.0464). The critical curves (LV and LL) are plotted with tick full and dashed lines and the UCEPs are drawn with triangles.

Table 7
AADP, % and AADY, % for the CO_2 + 2,4-DMP binary system with average values of BIPs.

EoS	GEOS		PR		SRK	
BIPs	k_{12}	l_{12}	k_{12}	l_{12}	k_{12}	l_{12}
	0.0165	0.0226	0.0499	0.0389	0.0569	0.0388
T/K	AADP/ %	AADY/ %	AADP/ %	AADY/ %	AADP/ %	AADY/ %
323.15	2.40	0.79	1.46	0.58	1.18	0.54
343.15	1.95	1.90	1.25	1.06	1.15	1.00
363.15	1.70	3.89	1.47	1.69	1.39	1.39
383.15	2.27	4.79	1.18	2.38	0.88	1.95

the optimized binary interaction parameters (BIPs: k_{ij} = 0.0165; l_{ij} = 0.0226) and the LL critical curve, the UCEP, and LLV line are not shown to have visible plots.

In Fig. 6 are compared the results for the PR EoS with the optimized values of BIPs (k_{ij} = 0.0499; l_{ij} = 0.0389). The UCEP is located at very low temperature and pressure (173.22 K and 0.46 bar) and it was only shown to point out that it cannot be observed due to the formation of solid phase. The enlargement of Fig. 6 (a) is shown in the Supplementary Information as Fig. 14S, while Fig. 7 depicts the comparison of the critical experimental data and the SRK equation of state with the average values of BIPs (k_{ij} = 0.0569; l_{ij} = 0.0388). In Fig. 7 (c), the projection of the LLV line is also shown. The AADP, % and AADY, % are slightly larger for the average values of the BIPs, as can be seen in Table 7, compared with the regression results. The isothermal experimental data, the correlation results, and the calculations with the average values of the BIPs are compared and plotted in Figs. 15S (GEOS), 16S (PR), and 17S (SRK). The differences between the representations with the optimized values of the BIPs and their average values are very small and therefore hardly visible.

As mentioned in the Modeling section, for the PR EoS, the binary interaction parameters were simultaneously fitted to all four isotherms using flash calculations. Thus, the BIPs are k_{12} = 0.060390 and l_{12} = 0.042365, while the AADP is 1.91% and AADY is 1.41%. This

approach improved marginally the LV critical curve (Fig. 6 and 14S.) and the vapor-liquid calculations (Fig. 16S).

In some recent papers [16,17] it was shown that systems containing carbon dioxide and branched alkanes or cycloalkanes can be successfully correlated by utilizing a temperature-dependent binary interaction parameter. Therefore, in the last part of this study we present our results using a k_{ij} that is temperature-dependent and a constant l_{ij} for all three models considered.

4.4. GEOS, PR and SRK results using a temperature-dependent k_{ij} and a constant l_{ij}

The function used for the temperature-dependent k_{ij} is similar with that described in [64]:

$$k_{ij} = k^{\infty} + k' \bullet e^{-\frac{T}{T^*}} \quad (27)$$

where $k^{\infty} = 0.01$, $k' = 0.05$, and $T^* = 304.21$ K (the critical temperature of carbon dioxide).

The second binary interaction parameter, l_{ij}, was determined by a trial-and-error procedure, and their values are 0.0701 for GEOS, 0.0640 for PR, and 0.0464 for SRK. The calculation results using the temperature-dependent k_{ij} and the constant l_{ij} are shown in Fig. 5 (GEOS), 6 and 14S (PR), and 7 (SRK) for the critical behavior and in Figs. 15S, 16S, and 17S for the isothermal data. The most significant improvement was obtained for the P–T, P–X_1, and T–X_1 projections in the case of GEOS model compared with the average BIPs' calculations (Fig. 5, dashed lines). However, even though the value of the CPM (120.95 bar) is nearer to the experimental one (121.4 bar), the corresponding critical composition is much smaller. Therefore, in the pressure-compositions diagrams (Fig. 15S), the vapor curves are located at lower compositions in CO_2. For the PR (Fig. 6, purple dashed lines) and SRK (Fig. 7, dark green dashed lines) EoSs the critical behavior is similar and better matched than using the average values of BIPs. It should be remarked that the liquid phase compositions are underestimated for both PR and SRK EoSs in the P–X_1, Y_1 diagrams (Fig. 16S and 17S). The AADP (%) and AADY (%) for the three models with the temperature-dependent k_{ij} and the constant l_{ij} are reported in Table 1S, and their values are reasonable.

5. Conclusions

Vapor–liquid equilibrium data at constant temperatures and VL critical data are reported for the first time for the CO_2 + 2,4-DMP binary system. The experiments were performed in a visual HP static-analytic installation. Pressure – compositions diagrams were measured at 323.15 K, 343.15 K, 363.15 K, and 383.15 K and pressures ranging between 10.4 and 120.4 bar. The vapor–liquid critical curve (pressures, temperatures, CO_2 compositions) was measured up to the maximum critical pressure of 121.4 bar and the greatest temperature of 422.35 K.

The GEOS, Peng–Robinson, and Soave–Redlich–Kwong EoSs together with one- and two-conventional parameters mixing rules were used to successfully model the phase behavior of the CO_2 + 2,4-DMP system.

Declaration of Competing Interest

The authors declare that they have no known competing financial interests or personal relationships that could have appeared to influence the work reported in this paper.

Data availability

Data will be made available on request.

Acknowledgment

"This work was supported by a grant of Ministry of Research, Innovation, and Digitization, CNCS - UEFISCDI, project number PN-III-P4-PCE-2021–0717, within PNCDI III".

Appendix A. Supporting information

Supplementary data associated with this article can be found in the online version at doi:10.1016/j.supflu.2023.105941.

References

[1] S. Sima, A.V. Crișciu, C. Secuianu, Phase behavior of carbon dioxide + isobutanol and carbon dioxide + tert-butanol binary systems, Energies 15 (2022) 2625, https://doi.org/10.3390/en15072625.
[2] S. Sima, C. Secuianu, The effect of functional groups on the phase behavior of carbon dioxide binaries and their role in CCS, Molecules 26 (2021) 3733, https://doi.org/10.3390/molecules26123733.
[3] S. M.S. Ioniță, M. Cismondi, C. Secuianu, Phase equilibria for the carbon dioxide + cyclopentane + cyclohexane system at high pressures, Rev. Roum. Chim. 66 (2021) 303–308, https://doi.org/10.33224/rrch.2021.66.3.11.
[4] S.Z. Al Ghafri, G.C. Maitland, J.P.M. Trusler, Experimental and modeling study of the phase behavior of synthetic crude oil+CO_2, Fluid Phase Equilib. 365 (2014) 20–40, https://doi.org/10.1016/j.fluid.2013.12.018.
[5] J.F.R. Yanes, F. Montel, J.L. Daridon, Fluid phase equilibria in asymmetric model systems. Part II: CO_2 + 2,2,4,4,6,8,8-heptamethylnonane, J. Supercrit. Fluids 189 (2022), 105721, https://doi.org/10.1016/j.supflu.2022.105721.
[6] J.-L. Daridon, F. Montel, D.V. Nichita, J. Pauly, Fluid-fluid and fluid-solid phase equilibria in carbon dioxide + waxy systems 1. CO_2 + n-C17, Fluid Phase Equilib. 538 (2021), 113023, https://doi.org/10.1016/j.fluid.2021.113023.
[7] R. Neerup, I.A. Løge, K. Helgason, S.Ó. Snæbjörnsdóttir, B. Sigfússon, J. B. Svendsen, N.T. Rosted, P. Blinksbjerg, J. Kappel, R. Rørtveit, S. Polak, N. Felbab, R. Holmer, A. Arora, J. Andersen, B.B. Jensen, S.N.B. Villadsen, G.M. Kontogeorgis, P.L. Fosbøl, A call for standards in the CO_2 value chain, Environ. Sci. Technol. 56 (2022) 17502–17505, https://doi.org/10.1021/acs.est.2c08119.
[8] J.-C. de Hemptinne, G.M. Kontogeorgis, R. Dohrn, I.G. Economou, A. ten Kate, S. Kuitunen, L. Fele Žilnik, M.G. De Angelis, V. Vesovic, A view on the future of applied thermodynamics, Ind. Eng. Chem. Res. 61 (2022) 14664–14680, https://doi.org/10.1021/acs.iecr.2c01906.
[9] G.M. Kontogeorgis, R. Dohrn, I.G. Economou, J.-C. de Hemptinne, A. ten Kate, S. Kuitunen, M. Mooijer, L.F. Žilnik, V. Vesovic, Industrial requirements for thermodynamic and transport properties: 2020, Ind. Eng. Chem. Res. 60 (2021) 4987–5013, https://doi.org/10.1021/acs.iecr.0c05356.
[10] I.G. Economou, G.M. Kontogeorgis, R. Dohrn, J.C. de Hemptinne, Advances in thermodynamics for chemical process and product design, Chem. Eng. Res. Des. 92 (2014) 2793–2794, https://doi.org/10.1016/j.cherd.2014.10.021.
[11] S. Peper, J.M.S. Fonseca, R. Dohrn, High-pressure fluid-phase equilibria: trends, recent developments, and systems investigated (2009–2012, Fluid Phase Equilib. 484 (2019) 126–224, https://doi.org/10.1016/j.fluid.2018.10.007.
[12] J.M.S. Fonseca, R. Dohrn, S. Peper, High-pressure fluid-phase equilibria: experimental methods and systems investigated (2005–2008, Fluid Phase Equilib. 300 (2011) 1–69, https://doi.org/10.1016/j.fluid.2010.09.017.
[13] R. Dohrn, S. Peper, J.M.S. Fonseca, High-pressure fluid-phase equilibria: experimental methods and systems investigated (2000–2004, Fluid Phase Equilib. 288 (2010) 1–54, https://doi.org/10.1016/j.fluid.2009.08.008.
[14] M. Christov, R. Dohrn, High-pressure fluid phase equilibria: experimental methods and systems investigated (1994–1999), Fluid Phase Equilib. 202 (2002) 153–218, https://doi.org/10.1016/S0378-3812(02)00096-1.
[15] R. Dohrn, G. Brunner, High-pressure fluid-phase equilibria: experimental methods and systems investigated (1988–1993), Fluid Phase Equilib. 106 (1995) 213–282, https://doi.org/10.1016/0378-3812(95)02703-H.
[16] S. Zid, J.-P. Bazile, J.-L. Daridon, J.-N. Jaubert, J.-L. Havet, M. Debacq, S. Vitu, High-pressure phase equilibria measurements of the carbon dioxide + cycloheptane binary system, J. Chem. Eng. Data 67 (2022) 176–181, https://doi.org/10.1021/acs.jced.1c00848.
[17] S. Zid, J.-P. Bazile, J.-L. Daridon, A. Piña-Martinez, J.-N. Jaubert, S. Vitu, Fluid phase equilibria for the CO_2 + 2,3-dimethylbutane binary system from 291.9 K to 373.1 K, J. Supercrit. Fluids 179 (2022), 105387, https://doi.org/10.1016/j.supflu.2021.105387.
[18] S. Sima, M. Cismondi, C. Secuianu, High-pressure phase equilibrium for carbon dioxide + ethyl n-butyrate binary system, J. Chem. Eng. Data 66 (2021) 4094–4102, https://doi.org/10.1021/acs.jced.1c00319.
[19] N.G. Tassin, S.B. Rodríguez Reartes, M. Cismondi, New correlations for prediction of high-pressure phase equilibria of n-alkane mixtures with the RKPR EoS: back from the use of lij (Repulsive) interaction parameters, J. Chem. Eng. Data 64 (2019) 2093–2109, https://doi.org/10.1021/acs.jced.8b01050.
[20] J. Friedrich, Near-infrared Spectroscopical Studies on the Phase Behavior and the Association of 3-hexanol, 3-methyl-3-pentanol in CO_2 and CClF3 and of 1-Octadecanol in CO_2 (Ph.D. Thesis), Ruhr-Universität Bochum,, Bochum, Germany, 1988, pp. 1–230 (Ph.D. Thesis).

[21] M. Ash, I. Ash. Handbook of Solvents, third ed., Synapse Information Resources, Inc.,, 2018.
[22] T. Kozaki, S. Takeya, R. Ohmura, Phase equilibrium and crystallographic structures of clathrate hydrates formed in methane + 2,2-dimethylpentane + water system, J. Chem. Eng. Data 53 (2008) 2820–2823, https://doi.org/10.1021/je800552k.
[23] A.A. Atamas, S.W. de Leeuw, H.M. Cuppen, A method distinguishing between guest molecules that can form sI, sII, and sH hydrogen clathrates, RSC Adv. 5 (2015) 26376–26382, https://doi.org/10.1039/C5RA03175C.
[24] G. Soave, Equilibrium constants from a modified Redlich-Kwong equation of state, Chem. Eng. Sci. 27 (1972) 1197–1203, https://doi.org/10.1016/0009-2509(72)80096-4.
[25] D.Y. Peng, D.B. Robinson, A new two-constant equation of state, Ind. Eng. Chem. Fundam. 15 (1976) 59–64, https://doi.org/10.1021/i160057a011.
[26] D. Geana, NEW state equation for fluids.3. Generalization of the cubic equations of state of the Vanderwaals type, Rev. De. Chim. 38 (1987) 975–979.
[27] D. Geana, N.E.W. FLUID, State equation.2. Application to the phase-equilibrium calculus, Rev. De. Chim. 37 (1986) 951–959.
[28] D. Geana, New equation of state for fluids.1. Application to pvt calculi for pure fluids, Rev. De. Chim. 37 (1986) 303–309.
[29] N.G. Tassin, S.B. Rodríguez Reartes, M. Cismondi, Activity coefficients in nearly athermal mixtures predicted from equations of state: don't blame the cubic when it is the lack of a third parameter!, Fluid Phase Equilib. 522 (2020), 112753, https://doi.org/10.1016/j.fluid.2020.112753.
[30] R. Privat, J.-N. Jaubert, The state of the art of cubic equations of state with temperature-dependent binary interaction coefficients: from correlation to prediction, Fluid Phase Equilib. 567 (2023), 113697, https://doi.org/10.1016/j.fluid.2022.113697.
[31] J.N. Jaubert, R. Privat, Relationship between the binary interaction parameters (kij) of the Peng-Robinson and those of the Soave-Redlich-Kwong equations of state: Application to the definition of the PR2SRK model, Fluid Phase Equilib. 295 (2010) 26–37, https://doi.org/10.1016/j.fluid.2010.03.037.
[32] J. Jaubert, R. Privat, F. Mutelet, Predicting the phase equilibria of synthetic petroleum fluids with the PPR78 approach, AIChE J. 56 (2010) 3225–3235, https://doi.org/10.1002/aic.12232.
[33] G.M. Kontogeorgis, R. Privat, J.N. Jaubert, Taking another look at the van der waals equation of state-almost 150 years later, J. Chem. Eng. Data 64 (2019) 4619–4637, https://doi.org/10.1021/acs.jced.9b00264.
[34] I. Polishuk, M. Katz, N. Pavlov, Prediction of phase equilibria in the systems carbon dioxide (1)–fatty acids (2) by two cubic EOS models and classical mixing rules without binary adjustable parameters, Fluid Phase Equilib. 289 (2010) 90–93, https://doi.org/10.1016/j.fluid.2009.11.021.
[35] I. Polishuk, An empirical modification of classical mixing rule for the cohesive parameter: the triple interactions in binary systems considered, Ind. Eng. Chem. Res. 49 (2010) 4989–4994, https://doi.org/10.1021/ie100138h.
[36] F. Mutelet, S. Vitu, R. Privat, J.-N. Jaubert, Solubility of CO_2 in branched alkanes in order to extend the PPR78 model (predictive 1978, Peng–Robinson EOS with temperature-dependent kij calculated through a group contribution method) to such systems, Fluid Phase Equilib. 238 (2005) 157–168, https://doi.org/10.1016/j.fluid.2005.10.001.
[37] S. Vitu, R. Privat, J.-N. Jaubert, F. Mutelet, Predicting the phase equilibria of CO_2+ hydrocarbon systems with the PPR78 model (PR EOS and kij calculated through a group contribution method, J. Supercrit. Fluids 45 (2008) 1–26, https://doi.org/10.1016/j.supflu.2007.11.015.
[38] J.-N. Jaubert, F. Mutelet, VLE predictions with the Peng–Robinson equation of state and temperature dependent kij calculated through a group contribution method, Fluid Phase Equilib. 224 (2004) 285–304, https://doi.org/10.1016/j.fluid.2004.06.059.
[39] P.H. van Konynenburg, R.L. Scott, J.S. Rowlinson, Critical lines and phase equilibria in binary van der Waals mixtures, Philos. Trans. R. Soc. Lond. Ser. A, Math. Phys. Sci. 298 (1980) 495–540, https://doi.org/10.1098/rsta.1980.0266.
[40] R. Privat, J.N. Jaubert, Classification of global fluid-phase equilibrium behaviors in binary systems, Chem. Eng. Res. Des. 91 (2013) 1807–1839, https://doi.org/10.1016/j.cherd.2013.06.026.
[41] M.M. Miller, K.D. Luks, Observations on the multiphase equilibria behavior of CO_2-rich and ethane-rich mixtures, Fluid Phase Equilib. 44 (1989) 295–304, https://doi.org/10.1016/0378-3812(89)80059-7.
[42] C. Secuianu, V. Feroiu, D. Geană, High-pressure vapor−liquid equilibria in the system carbon dioxide and 2-propanol at temperatures from 293.25 K to 323.15 K, J. Chem. Eng. Data 48 (2003) 1384–1386, https://doi.org/10.1021/je034027k.
[43] C. Secuianu, V. Feroiu, D. Geană, High-pressure phase equilibria for the carbon dioxide + methanol and carbon dioxide + isopropanol systems, Rev. De. Chim. 54 (2003) 874–879.
[44] S. Sima, V. Feroiu, D. Geană, New high pressure vapor–liquid equilibrium data and density predictions for carbon dioxide+ethyl acetate system, Fluid Phase Equilib. 325 (2012) 45–52, https://doi.org/10.1016/j.fluid.2012.03.028.
[45] S. Sima, V. Feroiu, D. Geană, New high pressure vapor–liquid equilibrium and density predictions for the carbon dioxide + ethanol system, J. Chem. Eng. Data 56 (2011) 5052–5059, https://doi.org/10.1021/je2008186.
[46] S. Peper, R. Dohrn, Sampling from fluid mixtures under high pressure: review, case study and evaluation, J. Supercrit. Fluids 66 (2012) 2–15, https://doi.org/10.1016/j.supflu.2011.09.021.
[47] P. Guilbot, A. Valtz, H. Legendre, D. Richon, Rapid on-line sampler-injector: a reliable tool for HT-HP sampling and on-line GC analysis, Analusis 28 (2000) 426–431.
[48] S. Sima, C. Secuianu, D.V. Nichita, High-pressure phase equilibria of carbon dioxide + 1,4-dioxane binary system, Fluid Phase Equilib. 547 (2021), 113181, https://doi.org/10.1016/j.fluid.2021.113181.
[49] S. Sima, C. Secuianu, V. Feroiu, S. Ioniță, D. Geană, High-pressure phase equilibria of carbon dioxide + 2-octanol binary system, Fluid Phase Equilib. 510 (2020), https://doi.org/10.1016/j.fluid.2020.112487.
[50] S. Sima, C. Secuianu, V. Feroiu, Phase equilibria of CO_2 + 1,2-dimethoxyethane at high-pressures, Fluid Phase Equilib. 458 (2018) 47–57, https://doi.org/10.1016/j.fluid.2017.11.008.
[51] C. Secuianu, S. Ioniţə, V. Feroiu, D. Geanə, High pressures phase equilibria of (carbon dioxide + 1-undecanol) system and their potential role in carbon capture and storage, J. Chem. Thermodyn. 93 (2016) 360–373, https://doi.org/10.1016/j.jct.2015.08.005.
[52] C. Secuianu, V. Feroiu, D. Geană, Phase behavior of the carbon dioxide + 1-dodecanol system at high pressures, Fluid Phase Equilib. 428 (2016) 62–75, https://doi.org/10.1016/j.fluid.2016.06.014.
[53] S. Sima, J.M. Milanesio, J.I. Ramello, M. Cismondi, C. Secuianu, V. Feroiu, D. Geanə, The effect of the naphthenic ring on the VLE of (carbon dioxide + alkane) mixtures, J. Chem. Thermodyn. 93 (2016) 374–385, https://doi.org/10.1016/j.jct.2015.07.018.
[54] E.-J. Choi, S.-D. Yeo, Critical properties for carbon dioxide + n-alkane mixtures using a variable-volume view cell, J. Chem. Eng. Data 43 (1998) 714–716, https://doi.org/10.1021/je9800297.
[55] C. Secuianu, V. Feroiu, D. Geană, Phase behavior for carbon dioxide + methanol system: experimental measurements and modeling with a cubic equation of state, Intern. J. Liq. State Sci. 2 (2010) 1–14.
[56] R. Privat, J.N. Jaubert, PPR78, a thermodynamic model for the prediction of petroleum fluidphase behaviour, In: Proceedings of the 2011 - 37th Conference on Phase Equilibria, 2011.
[57] A. Pina-Martinez, R. Privat, J.N. Jaubert, D.Y. Peng, Updated versions of the generalized Soave α-function suitable for the Redlich-Kwong and Peng-Robinson equations of state, Fluid Phase Equilib. 485 (2019) 264–269, https://doi.org/10.1016/j.fluid.2018.12.007.
[58] S.b.A. Design Institute for Physical Properties, DIPPR Project 801 - Full Version, in, Design Institute for Physical Property Research/AIChE.
[59] A. Piña-Martinez, R. Privat, S. Lasala, G. Soave, J.N. Jaubert, Search for the optimal expression of the volumetric dependence of the attractive contribution in cubic equations of state, Fluid Phase Equilib. 522 (2020), https://doi.org/10.1016/j.fluid.2020.112750.
[60] J.N. Jaubert, Y. Le Guennec, A. Piña-Martinez, N. Ramirez-Velez, S. Lasala, B. Schmid, I.K. Nikolaidis, I.G. Economou, R. Privat, Benchmark database containing binary-system-high-quality-certified data for cross-comparing thermodynamic models and assessing their accuracy, Ind. Eng. Chem. Res. 59 (2020) 14981–15027, https://doi.org/10.1021/acs.iecr.0c01734.
[61] P. Englezos, N. Kalogerakis, P. Raj Bishnoi, A systematic approach for the efficient estimation of interaction parameters in equations of state using binary vle data, Can. J. Chem. Eng. 71 (1993) 322–326, https://doi.org/10.1002/cjce.5450710220.
[62] J. Brest, M.S. Maučec, Self-adaptive differential evolution algorithm using population size reduction and three strategies, Soft Comput. 15 (2011) 2157–2174, https://doi.org/10.1007/s00500-010-0644-5.
[63] J. Brest, V. Zumer, M.S. Maucec, Self-Adaptive Differential Evolution Algorithm in Constrained Real-Parameter Optimization, In: Proceedings of the 2006 IEEE International Conference on Evolutionary Computation, 2006, pp. 215–222.
[64] M. Cismondi, J.M. Mollerup, M.S. Zabaloy, Equation of state modeling of the phase equilibria of asymmetric CO_2+n-alkane binary systems using mixing rules cubic with respect to mole fraction, J. Supercrit. Fluids 55 (2010) 671–681, https://doi.org/10.1016/j.supflu.2010.10.007.
[65] D.R. Geana, Liviu, Phase equilibria database and calculation program for pure components systems and mixtures, In: Proceedings of the Romanian International Conference on Chemistry and Chemical Engineering - RICCCE XIV, Bucharest, Romnaia, 2005, pp. 170–178.
[66] M. Cismondi, J. Mollerup, Development and application of a three-parameter RK–PR equation of state, Fluid Phase Equilib. 232 (2005) 74–89, https://doi.org/10.1016/j.fluid.2005.03.020.
[67] M. Cismondi, E.A. Brignole, J. Mollerup, Rescaling of three-parameter equations of state: PC-SAFT and SPHCT, Fluid Phase Equilib. 234 (2005) 108–121, https://doi.org/10.1016/j.fluid.2005.06.002.
[68] M. Cismondi, M.L. Michelsen, Global phase equilibrium calculations: critical lines, critical end points and liquid–liquid–vapour equilibrium in binary mixtures, J. Supercrit. Fluids 39 (2007) 287–295, https://doi.org/10.1016/j.supflu.2006.03.011.
[69] R.A. Heidemann, A.M. Khalil, The calculation of critical points, AIChE J. 26 (1980) 769–779, https://doi.org/10.1002/aic.690260510.
[70] R. Stockfleth, R. Dohrn, An algorithm for calculating critical points in multicomponent mixtures which can easily be implemented in existing programs to calculate phase equilibria, Fluid Phase Equilib. 145 (1998) 43–52, https://doi.org/10.1016/S0378-3812(97)00225-2.
[71] D.V. Nichita, S. Gomez, Efficient and reliable mixture critical points calculation by global optimization, Fluid Phase Equilib. 291 (2010) 125–140, https://doi.org/10.1016/j.fluid.2009.12.023.
[72] S.Z.S. Al Ghafri, E. Forte, G.C. Maitland, J.J. Rodriguez-Henríquez, J.P.M. Trusler, Experimental and modeling study of the phase behavior of (Methane + CO_2 + Water) mixtures, J. Phys. Chem. B 118 (2014) 14461–14478, https://doi.org/10.1021/jp509678g.